Fungi-derived xylindein: effect of purity on optical and electronic properties

Gregory Giesbers, Taylor Krueger, Jonathan Van Schenck, Ray Van Court, Jeffrey Morré, Chong Fang, Sara Robinson, Oksana Ostroverkhova

Oregon State University, Corvallis, OR, United States

ABSTRACT

We present a study of optical and electronic properties of solutions and films based on the fungi-derived pigment xylindein, extracted from decaying wood and processed without and with a simple purification step ("ethanol wash"). The "post-wash" xylindein solutions exhibited considerably lower absorption in the ultraviolet spectral range and dramatically reduced photoluminescence below 600 nm, due to removal of contaminants most likely to be fungal secondary metabolites. The "post-wash" xylindein-based films were characterized by two orders of magnitude higher charge carrier mobilities as compared to "pre-wash" samples. This underlines the importance of minimizing contaminants that disrupt the conductive xylindein network in xylindein-based electronic devices.

INTRODUCTION

Organic semiconductors are of considerable interest due to their low cost, tunability, and solution processability [1]. Over the past decade, there has been a growing interest in naturally sourced and sustainable organic materials for (opto)electronic applications [2]. Naturally derived pigments exhibit extraordinary stability with respect to a variety of environmental factors [3]–[5], which is important since low stability is one of the bottlenecks preventing wide commercialization of organic semiconductor devices. Additionally, when implemented in electronic devices some of the pigments performed surprisingly well in spite of an only partially conjugated core structure [3], [6]. One of the promising naturally sourced pigments for organic electronics is xylindein, secreted by the non-pathogenic wood-staining fungi *Chlorociboria (C.) aeruginosa* or *C. aeruginascens*. We recently reported the optical and electronic properties of xylindein [7], [8], amorphous films of which exhibited electron mobilities of up to 0.4 cm^2/(Vs). Furthermore, xylindein considerably outperformed benchmark organic semiconductors in terms of the photostability in air [8]. Similar to many natural products, naturally sourced

xylindein requires extraction from liquid cultures and subsequent purification. Purification procedures may lead to a low yield of the purified material, thus reducing its utility for device applications. Depending on the purification protocol, this may become a time-consuming and costly process. Therefore, it is important to understand how various degrees of purification affect electronic properties and to develop less time-consuming and wasteful purification methods. In this paper, we implement a simple purification method and compare optical and electronic properties of xylindein before and after purification.

EXPERIMENTAL

Xylindein extraction

Xylindein was harvested from wood collected at Tidewater, Oregon, USA (Fig. 1(a)). Appropriate wood was identified by the signature blue-green color produced by *Chrlorociboria* species, which is unique across several kingdoms. The *Chlorociboria* species responsible for staining the wood was identified as *C. aeruginosa* through DNA extraction and Sanger sequencing of the ITS region, followed by GenBank Megablast comparison [9]. The collected wood was crushed into 2-3 mm fragments and the powder was placed in a 500 mL flask so that the bottom of the flask was evenly covered. 100 mL of dichloromethane (DCM) was poured into the flask and the contents were stirred on a magnetic plate for one hour before filtration as described in Ref. [10]. The solid crude xylindein was collected from evaporated DCM solution. When used without further processing, it will be referred to as "pre-wash" sample and its properties will be compared to a "post-wash" sample prepared as described below. The solid xylindein prepared as the "pre-wash" xylindein was sonicated in ethanol to form a suspension of xylindein aggregates. The ethanol solution was passed through a 0.45 μm PTFE filter, followed by multiple passes of clean ethanol through the filter to remove contaminants; the solution of contaminants in ethanol will be referred to as "ethanol wash" (Fig. 1(b)). The xylindein was removed from the filter with DCM, and solvents were evaporated to yield "post-wash" xylindein powder. The "post-wash" xylindein re-dissolved in DCM is shown in Fig. 1(c) and xylindein molecular structure in Fig. 1(d).
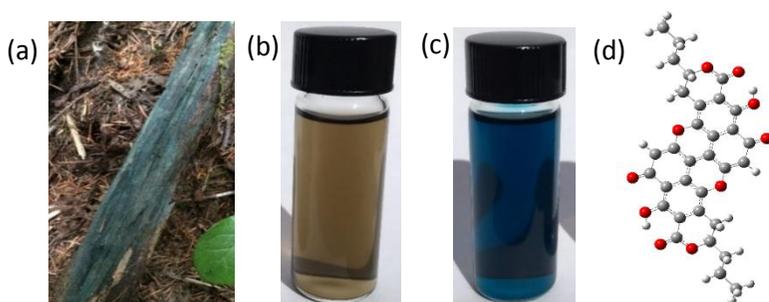

Figure 1: (a) *C. aeruginosa* producing blue-green pigment xylindein on the decaying wood. (b) "Ethanol wash" sample - contaminants in ethanol, washed away from xylindein extracted from the wood. (c) "Post-wash" sample - purified xylindein solution in DCM, after ethanol wash. (d) Molecular structure of xylindein.

Mass spectrometry

Analyses were performed on a Shimadzu HPLC (Columbia, MD) coupled to a Waters Synapt HDRMS time of flight mass spectrometer (Milford, MA). The MS was operated in negative ion mode, 80-1000 m/z scan range, 1 second scan time. A binary gradient and a 2.5 mm 2.1 x 50 mm c XTerra® MSC8 column (Waters, Milford, MA) were used for analytical separation. Solvent A consisted of MS grade water (Fisher Scientific, Fairlawn, NJ) and 0.1% formic acid (EMD Millipore Corporation, Billerica, MA) and solvent B consisted of MS grade acetonitrile (Fisher Scientific, Fairlawn, NJ) and 0.1% formic acid. "Pre-wash" and "post-wash" xylindein samples in DCM, along with the "ethanol wash" sample, were tested at 1:30 dilution.

Sample preparation

Xylindein powder was dissolved into DCM to form solutions of concentration 10 mg/mL. For optical measurements, the solutions were further diluted with DCM to achieve appropriate optical density for the spectroscopic apparatus. Films were prepared by drop-casting the concentrated solution onto glass substrates with planar Al electrodes with a 50 µm gap. The substrates were patterned using conventional lift-off photolithography, and Al was deposited using a Veeco 7700 thermal evaporator. The drop-cast xylindein films were approximately 3-5 µm thick, as measured by an Alpha Step 500 profilometer.

Measurement procedures

The steady-state absorption measurements were taken using a Thermo Scientific Evolution 201 UV/Visible (UV/Vis) spectrophotometer at room temperature. The path length of the quartz cuvette (1-Q-1, Starna Cells, Inc.) used for the absorption measurements was 1 mm, and the OD for both the "pre-wash" and "post-wash" xylindein solutions was ~0.5 at 656 nm following a background/baseline measurement of pure DCM solvent.

The steady-state fluorescence measurements of the "pre-wash" and "post-wash" samples were performed using a Shimadzu RF-6000 Spectro Fluorophotometer at room temperature with 400 nm excitation. The path length of the 4-sided rectangular quartz cuvette used for the emission measurements was 5 mm. The excitation and emission slit-widths were both set to 5 nm. Additional fluorescence measurements were taken using an Ocean Optics USB2000-FLG spectrometer with 532 nm excitation from a frequency-doubled Nd:YVO$_4$ laser.

For measurements of current-voltage characteristics, voltage was applied to the samples using a Keithley 237 source-measure unit. Current was measured as a function of applied voltage in the 0-10 V range, under ambient conditions in the dark.

Density Functional Theory (DFT) calculations

In order to calculate the vertical transition energies for the two molecular tautomers of xylindein (Fig. 2), both configurations were optimized in the electronic ground state using DFT methods in Gaussian 16 [11]. The B3LYP functional with the basis set 6-311++G(d,p) and a polarizable continuum model for DCM solvent were used. The energies of vertical transitions into each of the first 50 excited states were then calculated

using time-dependent (TD)-DFT methods along with their associated oscillator strengths. Due to molecular symmetry, most of these vertical transitions are forbidden, leading to zero oscillator strength; all the allowed transitions are shown in Fig. 2.

RESULTS AND DISCUSSION

Effect of contaminants on optical properties

Figure 2 shows the optical absorption spectrum of a dilute solution of "post-wash" xylindein in DCM. The complicated structure of the S_0-S_1 part of the spectrum (600-750 nm) was analysed in our previous publication [8] and attributed to a joint contribution of two vibronic progressions resulting from two xylindein tautomers (Fig. 2), wherein tautomer 1 has the hydroxyl groups pointed toward the conjugated core and tautomer 2 has the hydroxyl groups pointed away from the core. In order to better understand the xylindein spectrum in the UV/Vis wavelength range, we calculated vertical energies and oscillator strengths of both tautomers for transitions from the ground state to several electronic excited states. Figure 2 shows the calculation result (which includes only the 0-0 lines and thus excludes the contribution of vibronic satellites to the spectra) superimposed with the experimental data. The calculated energies of the S_0-S_n transitions are slightly blue-shifted from the experimental values (e.g. by 10 and 18 nm, or 0.03 and 0.05 eV, for the S_0-S_1 transitions for the tautomers 1 and 2, respectively [8]). Nevertheless, the calculations help us understand what spectral features should be expected from xylindein molecules.
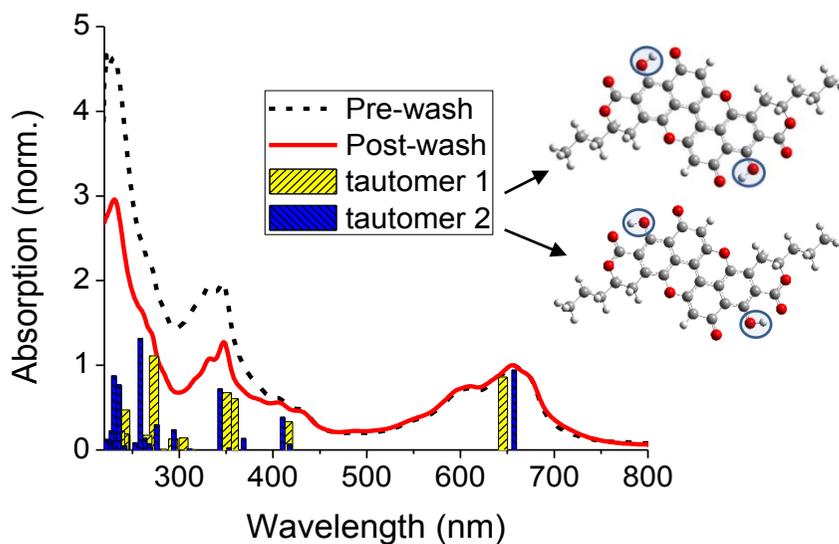

Figure 2: UV/Vis absorption spectra of xylindein before and after ethanol wash, overlaid with the 0-0 vertical transition energies determined from TD-DFT calculations for the two tautomers 1 (top) and 2 (bottom) of xylindein, shown on the right.

Figure 3 shows a comparison between the optical absorption spectra (a) and photoluminescence (PL) spectra (b) obtained from "pre-wash" and "post-wash" xylindein solutions. While the absorption in the 500-700 nm region corresponding to that from the

S_0-S_1 transition of xylindein remains unchanged, a dramatic reduction in the UV-absorbing species (which will be referred to as contaminants) was observed as a result of the ethanol wash (Figure 2). The PL of xylindein occurs in the ~680-800 nm wavelength region (Fig. 3(a)) and is very weak, with a quantum yield of <0.1% [8]. A considerably stronger PL was observed from contaminants in the "pre-wash" sample, occurring in the broad (400-600 nm) spectral region upon 400 nm excitation. The ethanol wash substantially reduced the PL from the contaminants by nearly 75% (relative to the "pre-wash" sample), although it did not eliminate it completely as seen from Fig. 3(b).
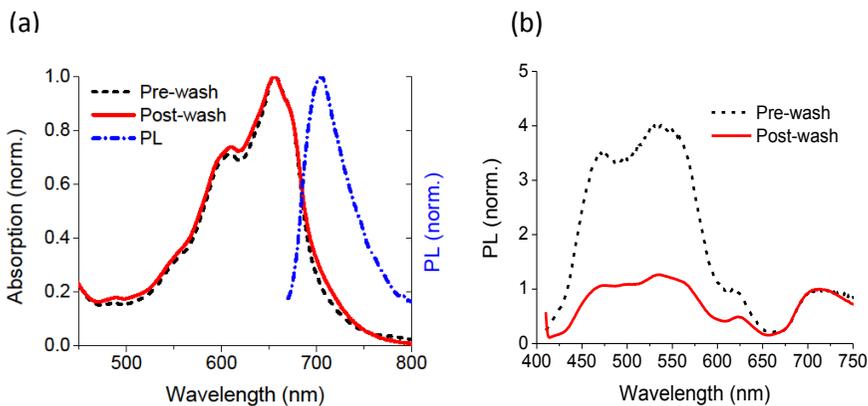
(a)

(b)

Figure 3: (a) Normalized absorption spectra before and after the ethanol wash, exhibiting negligible change in absorption in the spectral region corresponding to the S_0-S_1 excitation of xylindein. PL spectrum of xylindein obtained upon 532 nm excitation of the "post-wash" sample is also shown. (b) Emission spectra before and after ethanol wash upon 400 nm excitation, normalized at 712 nm, exhibiting a large discrepancy in PL from contaminants mainly responsible for emission below ~600 nm.

Effect of contaminants on electronic properties

Figure 4 shows a comparison between electronic properties of films made from "pre-wash" and "post-wash" xylindein solutions as described in the Experimental. An increase in the current of more than 2 orders of magnitude was observed in samples made with a "post-wash" xylindein. The electron mobilities were calculated from the space-charge-limited current (SCLC) regime of the I-V characteristics (when $I \sim V^2$), in the thin-film approximation [8], [12] (Eq. (1)).

$$j = \frac{2\mu_{eff}\epsilon\epsilon_0}{\pi}\frac{V^2}{L^2} \tag{1}$$

Here j is the linear current density, j = I/d, where I is the measured current and d is the length of the electrode. V is the applied voltage, L is the gap between the electrodes, ε_0 is the vacuum permittivity, ε is the dielectric constant (assumed to be equal to 3), and μ_{eff} is the effective electron mobility. The effective mobilities yielded 1.6 x 10^{-3}

cm^2/(Vs) and 0.19 cm^2/(Vs) in the "pre-wash" and "post-wash" samples, respectively. The relatively high charge carrier mobility in the amorphous films of the "post-wash" samples could be indicative of a beneficial interplay between the π–π stacking and hydrogen bonding [6], [13] which are both expected in a xylindein solid, for efficient charge transport. Films deposited from the "ethanol wash" solution of contaminants exhibited negligible conductivity.
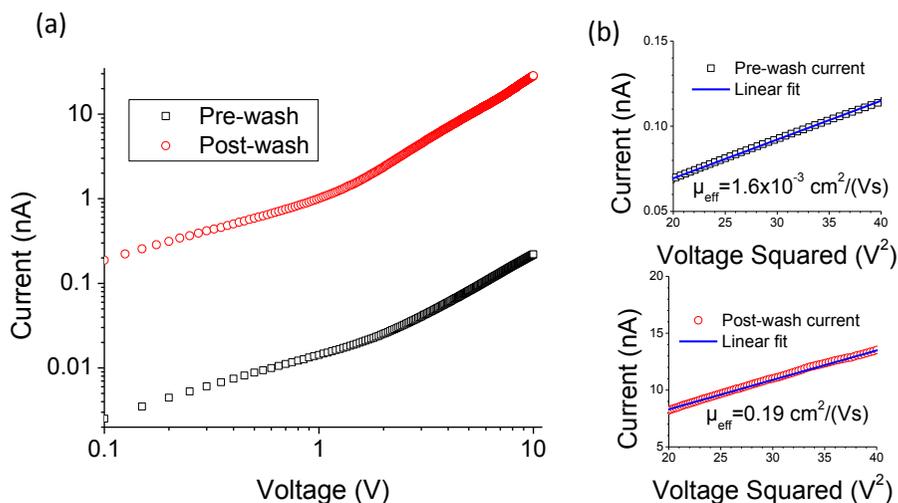

Figure 4: (a) Current-voltage (I-V) characteristics for the "pre-wash" and "post-wash" xylindein film on coplanar Al electrodes with a 50 µm gap, showing transition from the linear to the quadratic (SCLC) regime. (b) SCLC data from (a) replotted as I versus V^2 for the "pre-wash" (top) and "post-wash" (bottom) samples. Fits from which the effective mobilities were calculated are also included.

Nature and properties of contaminants

Next, we sought to understand the nature of contaminants that play such a dramatic role in conductive properties of xylindein-based films. Towards that goal, we analysed mass spectra of "pre-wash" and "post-wash" xylindein samples, as well as of the "ethanol wash" containing contaminants. Negative ion analysis showed clear differences in peaks between the "pre-wash" and "ethanol wash" samples when compared to the "post-wash" samples. An initial peak which eluted at retention time of ~2.3 min was present in the "pre-wash" and "ethanol wash" samples, but not in the "post-wash" xylindein sample (Fig. 5(a)). The dominant mass peak at this elution time, not present in the "post-wash" sample, had a mass of 227.0926. Xylindein was observed at 11.1 minutes at a mass of 567.1268, with a -4.1 ppm mass accuracy corresponding to the (M - H)$^-$ ion, in accordance with the molecular formula of $C_{32}H_{23}O_{10}$ [14], [15]. A further peak present in the "pre-wash" and "ethanol wash" samples, but greatly reduced in the "post-wash" sample was at ~12.9 min, associated with a dominant mass of 573.1976. At 13.1 min, the dominant mass peak in the "pre-wash" and "ethanol wash" samples, but not the "post-wash" sample, had a mass of 573.1713 (Fig. 5(b)). At ~15.7 min, multiple peaks were present in the "pre-wash" and "ethanol wash" samples, but not in the "post-wash"

sample. Most notable mass peaks that showed distinct differences between the "pre-wash" and "post-wash" samples were 349.2379, 368.3214, and 411.227. As there are several candidates for the responsible molecules, including various fungal secondary metabolites, information on the mass alone is not sufficient for reliable identification and the exact assignment will be performed in future studies. However, based on the optical and PL properties of these contaminants and the procedure leading to their effective removal, we hypothesize that these are polar molecules with a considerably reduced conjugation length as compared to that of xylindein.
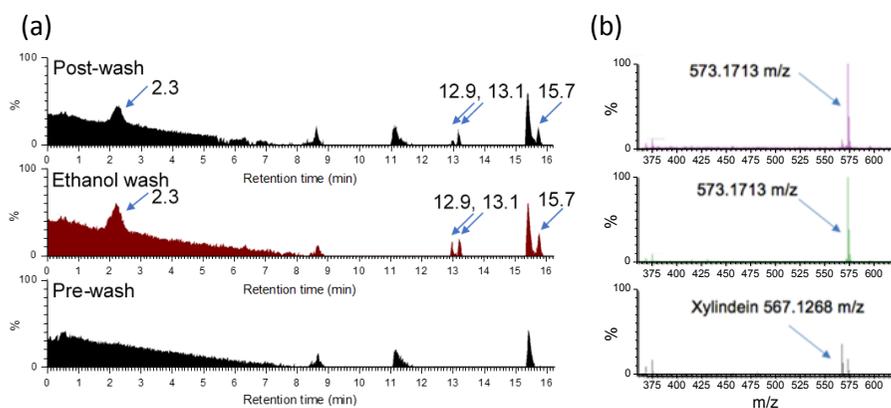

Figure 5: (a) Mass spectroscopy chromatogram of "pre-wash" and "post-wash" xylindein samples (top and bottom), as well as the "ethanol wash" (middle). Four peaks present in "pre-wash" and "ethanol wash" samples, with retention times (in minutes) denoted by arrows, were absent in the "post-wash" sample. (b) Masses at retention time of 13.1 min, including the peak corresponding to xylindein (highlighted in the "post-wash" sample, bottom). Also highlighted is the dominant contaminant peak with mass of 573.1713 m/z in the "pre-wash" (top) and "ethanol wash" (middle) samples.

Regardless of the exact molecular structures of the contaminants removed by the ethanol rinse, we surmise that they disrupt the conductive network of xylindein aggregates by introducing charge traps and non-conductive linkers. In particular, introduction of the fungi secondary metabolite molecules in the xylindein-based films would considerably disrupt both π–π stacking and hydrogen bonding between the xylindein molecules, which determine charge transport properties of xylindein films. To better understand the trade-off between a significantly improved electronic performance and the production costs of purification, more studies correlating purification protocols with subsequent effects on optical and electronic properties are necessary to quantify the corresponding changes in the charge carrier mobilities and in the mechanisms of conduction. These are currently underway and will be reported elsewhere.

CONCLUSIONS

Dramatic effects from an ethanol wash on the optical and electronic properties of the xylindein solution precursor and xylindein-based thin films, respectively, were observed. Considerably reduced UV absorption and PL at below 600 nm were obtained in "post-wash" solutions as compared to "pre-wash" solutions. These changes were correlated with a two orders of magnitude enhancement in charge carrier mobility in films drop-cast from "post-wash" solutions as compared to those from "pre-wash" solutions. Mass

spectrometry revealed several contributors, hypothesized to be fungal secondary metabolites, responsible for these observations. Removal of these molecules, which serve as contaminants in "pre-wash" xylindein-based devices that disrupt the $\pi-\pi$ stacking and hydrogen bonding between xylindein molecules, dramatically increases conductivity of the xylindein-based films. Studies correlating further purification protocols and electronic properties of xylindein-based films are underway.

ACKNOWLEDGMENTS

References:

[1]   O. Ostroverkhova, Chem. Rev. **116**, 13279 (2016).

[2]   M. Irimia-Vladu, Chem. Soc. Rev. **43**, 588 (2014).

[3]   M. Irimia-Vladu, E. D. Glowacki, P. A. Troshin, G. Schwabegger, L. Leonat, D. Susarova, O. Krystal, M. Ullah, Y. Kanbur, M. Bodea, V. Razumov, H. Sitter, S. Bauer, and N. S. Sariciftci, Adv. Mater. **24**, 375 (2012).

[4]   E. D. Glowacki, G. Voss, L. Leonat, M. Irmia-Vladu, S. Bauer, and N. S. Sariciftci, Isr. J. Chem. **52**, 540 (2012).

[5]   M. Dittmann, F. F. Graupner, B. Maerz, S. Oesterling, R. Devivie-Riedle, W. Zinth, M. Engelhard, and W. Luettke, Angew. Chemie - Int. Ed. **53**, 591 (2014).

[6]   E. D. Głowacki, M. Irimia-Vladu, S. Bauer, and N. S. Sariciftci, J. Mater. Chem. B **1**, 3742 (2013).

[7]   G. Giesbers, J. Van Schenck, S. V. Gutierrez, and S. Robinson, MRS Adv. **3**, 3459 (2018).

[8]   G. Giesbers, J. Van Schenck, A. Quinn, R. Van Court, S. Vega Gutierrez, S. Robinson, and O. Ostroverkhova, *submitted* (2019).

[9]   D. Benson, I. Karsch-Mizrachi, K. Clark, D. Lipman, J. Ostell, and E. Sayers, Nucleic Acids Res. **40**, D48 (2012).

[10]   S. C. Robinson, V. S. Gutierrez, R. A. Cespedes, N. Iroume, N. R. Vorland, A. McClelland, M. Huber, and S. Stanton, J. Coatings Technol. Res. **14**, 1107 (2017).

[11]   M. Frisch, G. Trucks, H. Schlegel, G. Scuseria, M. Robb, M. Cheeseman, G. Scalmani, V. Barone, G. Petersson, and H. Nakatsuii, X. Li, M. Caricato, A. V. Marenich, J. Bloino, B. G. Janesko, R. Gomperts, B. Mennucci, H. P. Hratchian, J. V. Ortiz, A. F. Izmaylov, J. L. Sonnenberg, D. Williams-Young, F. Ding, F. Lipparini, F. Egidi, J. Goings, B. Peng, A. Petrone, T. Henderson, D. Ranasinghe, V. G. Zakrzewski, J. Gao, N. Rega, G. Zheng, W. Liang, M. Hada, M. Ehara, K. Toyota, R. Fukuda, J. Hasegawa, M. Ishida, T. Nakajima, Y. Honda, O. Kitao, H. Nakai, T. Vreven, K. Throssell, J. A. Montgomery, Jr., J. E. Peralta, F. Ogliaro, M. J. Bearpark, J. J. Heyd, E. N. Brothers, K. N. Kudin, V. N. Staroverov, T. A. Keith, R. Kobayashi, J. Normand, K. Raghavachari, A. P. Rendell, J. C. Burant, S. S. Iyengar, J. Tomasi, M. Cossi, J. M. Millam, M. Klene, C. Adamo, R. Cammi, J. W. Ochterski, R. L. Martin, K. Morokuma, O. Farkas, J. B. Foresman, and D. J. Fox, Gaussian 16, Wallingford, CT (2016).

[12]   J. Day, A. D. Platt, S. Subramanian, J. E. Anthony, and O. Ostroverkhova, J. Appl. Phys. **105**,

103703 (2009).
[13]   N. Gospodinova and E. Tomšík, Prog. Polym. Sci. **43**, 33 (2015).
[14]   R. L. Edwards and N. Kale, Tetrahedron **21**, 2095 (1965).
[15]   Y. Saikawa, T. Watanabe, K. Hashimoto, and M. Nakata, Phytochemistry **55**, 237 (2000).